Generalized mean-field potential description for ferroelectric ordering in nematic liquid crystals

Byoungchoo Park* and J. W. Wu
Department of Physics, Ewha Womans University, Seoul 120-750, Korea

Hideo Takezoe
Department of Organic and Polymeric Materials, Tokyo Institute of Technology, O-okayama, Meguro-ku, Tokyo 152-8552, Japan
(Received 7 July 2000; published 26 January 2001)

Ferroelectric ordering in a nematic liquid crystal system is described using a generalized mean-field potential including effective potentials for both axial and polar interactions. From a self-consistent numerical analysis, a complete phase diagram is obtained as a function of the axial and polar interaction potential strengths. The obtained phase diagram exhibits not only the usual isotropic-nematic phase transition but also nematic-ferroelectric nematic and direct isotropic-ferroelectric nematic phase transitions with a tricritical point among the phases. The phase transition behaviors and the angular orientational distribution function of the molecules were investigated by studying the dependence of the polar and the axial order parameters on the reduced temperature. Moreover, the other polar order parameters responsible for second-harmonic generation (SHG) were also investigated in the generalized mean-field potential description. As a concrete example, we performed a quantitative analysis of the SHG signal reported previously in a lyotropic poly *L*-glutamate system, detailing the relationship between the angular distribution function and the order parameters based on our potential model. This clarifies the nature of the ferroelectric phase responsible for SHG in nematics.

DOI: 10.1103/PhysRevE.63.021707 PACS number(s): 61.30.Eb, 61.30.Gd, 68.08.−p

I. INTRODUCTION

Ferroelectricity and antiferroelectricity in liquid crystals (LC's) were respectively discovered in 1975 [1] and 1989 [2] in chiral smectic phases. In both cases, polar structure in a layer is realized by reducing symmetries through the introduction of chiral carbons into achiral systems. The second example of ferroelectric switching in liquid crystals was discovered in bent-core molecular systems [3], in which the characteristic packing of these molecules induces polar order in the layers. Thus these ferroelectric and antiferroelectric structures in LC's are improper, in the sense that dipole-dipole interaction does not play a major role in realizing the ferroelectric and antiferroelectric structures [4]. In contrast, the possibility for proper ferroelectricity in nematic LC's has been discussed because it attracted great interest both from fundamental and practical viewpoints [5–13].

Several theoretical studies of ferroelectricity in a nematic liquid crystal system were reported [5–9]. The authors of Ref. [5] theoretically examined the possibility that molecules with permanent dipole moments can form a ferroelectric nematic phase. They showed that electric dipolar interactions between disk-shaped molecules may lead to a ferroelectric phase in a mean-field theory, where the aspect ratio (d/l) dependent molecular interaction is introduced, with l the diameter along the cylindrical symmetry axis and d the diameter in a direction perpendicular to the axis. Wei and Patey [6] showed theoretically that dipolar forces can create an orientationally ordered liquid crystalline state, and that the existence of a ferroelectric nematic phase can be established in a strongly interacting dipolar spheres system using the molecular dynamic simulations. In their simulations, the angle-dependent pair distribution of the axially symmetric dipolar particles was expanded in terms of the radial distribution function with the parameters of the reduced density, the reduced temperature, and the reduced dipole moment. Baus and Colot [7] introduced an angular distribution function with two order parameters—the usual nematic axial order parameter and the ferroelectric polar order parameter along the director $(\hat{n})$, where nonspherical polar molecules were treated as hard ellipsoids of (d/l). Minimizing the free energy per molecule, they plotted the isotropic, usual nematic, and ferroelectric nematic phase diagrams as functions of the reduced dipole moment and the packing fraction for the given aspect ratios. The authors of Ref. [8] investigated the possibility of a ferroelectric phase transition in nematic polymers from the density functional approach. They introduced a Landau-type expansion of the corresponding free energy in powers of the macroscopic polarization P, and discussed the ferroelectric instability which manifested in the sign inversion of the familiar quadratic term $(T-T_c)P^2$. They showed that the ferroelectric instability temperature T_c is roughly proportional to the persistence length of the polymer. From an estimation of the instability temperature for the realistic values of the dipole strength, they explained why dipolar nematic polymers seem more likely to be ferroelectric than low molecular-weight nematic liquid crystals. Another interesting theoretical prediction was made by Lee and Lee [9]. By considering the dipole-dipole interaction and the hard-core repulsion in a mean-field model within the Onsager formalism, they showed that rodlike molecules can exhibit conventional isotropic-nematic, nematic-ferroelectric nematic, and direct isotropic-ferroelectric nematic transitions as scaled parameters such as the dipolar strength, density, and pressure are varied.

On the other hand, the ferroelectric behavior and the polar

*Author to whom correspondence should be addressed. Electronic address: bcpark@mm.ewha.ac.kr

structure characteristics in nematic liquid crystals were observed experimentally in a few polymeric systems, namely, the aromatic copolyester and the α-helical polypeptide. Furukawa and co-workers [10,11] and Watanabe *et al.* [12] reported second-harmonic generation (SHG) experimental observations where the polar ordering characteristics emerge as the degree of polymerization increases in the polar rodlike aromatic copolyester, consisting of 4-hydroxybenzoic acid and 6-hydroxy-2-naphthoic acid. Furthermore, in the SHG interferometry and the switching current measurements, Park *et al.* [13] reported a characteristic polar ferroelectric response upon the application of the electric field in a nematic liquid crystal, namely, a polar α-helix poly *L*-glutamate in a lyotropic cholesteric phase with the helical pitch of 1 μm, which was the first demonstration of the existence of ferroelectric cholesteric liquid crystalline phase. Takezoe and Watanabe [4] observed enhanced SHG from the helical state, when the SHG wavelength agrees with the optical pitch without applying an electric field.

The theoretical analyses introduced above are based on a simplified microscopic model of liquid crystalline molecule, and hence are not readily applicable to the explanation of the observed ferroelectric response in the complex liquid crystalline systems employed in experiments. In other words, most theoretical works introduce model molecular parameters such as the aspect ratio d/l, the reduced density, the reduced dipole moment, the packing fraction, the persistence length, etc. In fact, it is very hard to determine which parameters are important in describing the macroscopic liquid crystal phase responsible for the ferroelectric nematic behavior, because the model molecular parameters employed in the theoretical analysis cannot be unambiguously defined in a real complex liquid crystalline system. More importantly, in a theoretical analysis incorporating the model molecular parameters, the importance of the higher polar orders, related to the SHG response, has not been addressed. It is well known that SHG is a powerful tool to monitor the noncentrosymmetric structure of the sample system and is related to both $\langle P_1\rangle$ and $\langle P_3\rangle$ through the molecular hyperpolarizability β_{ijk}. Here $\langle P_i\rangle$ represents the thermodynamic orientational average of the Legendre polynomial of the ith order (see Sec. III for details).

From these considerations, we introduce a generalized mean-field potential incorporating both axial and polar effective interaction potentials, independent of the model molecular parameters, to describe the ferroelectric ordering in nematic liquid crystals. By employing a self-consistent numerical simulation, typical of the mean-field potential scheme, with effective interaction potentials as variables, we can examine the existence and nature of the stable macroscopic liquid crystalline phases. The nonvanishing value of the polar order parameter $\langle P_1\rangle$ will indicate the existence of the ferroelectric nematic phase, while the axial order parameter $\langle P_2\rangle$ will be nonzero for both the usual nematic and ferroelectric nematic phases.

In this paper, we performed a self-consistent numerical analysis of the mean-field potential, and obtained a complete phase diagram of the liquid crystalline molecular system as a function of the axial and the polar interaction potential strengths. The polar order parameters $\langle P_1\rangle$ and $\langle P_3\rangle$ were also obtained to relate the phases of a liquid crystalline molecular system with the SHG response. As an application of the mean-field potential analysis, we performed a quantitative analysis of the SHG signal reported previously [13] in a lyotropic poly *L*-glutamate system, detailing the relationship between the angular distribution function and the order parameters based on our potential model. The generalized mean-field theory is introduced in Sec. II. Based on the analysis developed in Sec. II the phase diagram, the phase transition behavior, and the SHG characteristics in the ferroelectric-nematic phase are presented in Sec. III. Finally, concluding remarks are made in Sec. IV.

II. GENERALIZED MEAN-FIELD POTENTIAL

Most of the previous theoretical works on ferroelectricity in nematic LC's [5–9] are based on models of the molecular system such as hard spherocylinders or ellipsoids with permanent dipoles with the mean-field potential. Instead of the microscopic molecular repulsive (or steric) and dipolar interactions [5–9], we simply introduce the effective mean-field potential for the ferroelectric nematic phase as follows:

$$V(\cos\theta) = V_{\text{axial}} + V_{\text{polar}},$$

$$V_{\text{axial}} = -v_2\langle P_2(\cos\theta)\rangle P_2(\cos\theta), \tag{1}$$

$$V_{\text{polar}} = -v_1\langle P_1(\cos\theta)\rangle P_1(\cos\theta),$$

where θ is the angle between the molecular direction and averaged molecular direction (director direction $\hat{n}$), v_2 and v_1 are the strength of the axial and the polar intermolecular interactions, respectively, and $\langle\,\rangle$ means the thermodynamic orientational average. Here $P_i(\cos\theta)$ represents the Legendre polynomial of the ith order, i.e., $P_1 = P_1(\cos\theta) = \cos\theta$, $P_2 = P_2(\cos\theta) = (3\cos^2\theta - 1)/2$, $P_3 = P_3(\cos\theta) = (5\cos^3\theta - 3\cos\theta)/2$, and so on. In Eq. (1), we assumed that both mesophase and individual molecules possess cylindrical symmetry in describing the molecular interactions, and neglected the potential terms related to the higher order Legendre polynomials [14,15] for simplicity. We would like to note that a form of the mean-field potential similar to Eq. (1) was introduced in theoretical descriptions for the ferromagnetic (nematic) systems [16–18]. This means that there exists a physical similarity between the ferroelectricity and ferromagnetism in nematics.

In Eq. (1), the effective nonpolar mean-field potential barrier V_{axial} is proportional to the nematic order parameter $\langle P_2\rangle$ and the effective polar mean-field potential V_{polar} is proportional to the polar order parameter $\langle P_1\rangle$. The polar coupling constant v_1 can be written as $v_1 \propto J_1^0 = m(d/l)(1 - \langle P_2\rangle/2)$ for semiflexible liquid crystalline polymers ($d/l \ll 1$) with the longitudinal dipole moment m [8]. If the coupling constant v_1 is zero, then $V(\cos\theta)$ reduces to the conventional nonpolar nematic mean-field potential (V_{axial}). This potential has two deep wells around the poles of the unit sphere of the orientation u, along the nematic director $\hat{n} = -\hat{n}$, and a barrier of height $v_2\langle P_2\rangle$ on its equator, penalizing the devia-

tions of θ from $\hat{n}$ [19,20]. Using V_{axial}, one can obtain traditional first-order isotropic-(nonpolar) nematic phase transition behaviors with the $\langle P_2 \rangle$ order parameter changing abruptly from 0 to ~0.43 (a universal value) by the numerical solution of the self-consistency equation [19,20]. If the coupling constant v_1 is negative, then $V(\cos\theta)$ indicates antiparallel dipolar interactions through the dimerization on the polar liquid crystals. Several interesting theoretical investigation were made to explain the strong dielectric anisotropies [21] or the abnormal phase transition behaviors for a given dipole strength of the LC molecule [22]. In this paper, however, we are mainly interested in ferroelectric nematics; thus we concentrate our attention on the case of positive v_1 for the formation of parallel dipole alignment in nematic liquid crystals.

The statistical mechanics gives the orientational distribution function in terms of the potential $V(\cos\theta)$ as

$$f(\cos\theta) = Z^{-1} \exp[-V(\cos\theta)/k_B T],$$
$$Z = \int_0^1 \exp[-V(\cos\theta)/k_B T] d(\cos\theta), \tag{2}$$

where k_B is the Boltzmann constant, T is the temperature, and Z is the partition function. With the distribution function f, one can calculate the average values $\langle \Omega(\cos\theta) \rangle$ of arbitrary physical parameter $\Omega(\cos\theta)$ of interest pertaining to the phase,

$$\langle \Omega(\cos\theta) \rangle = \int_0^1 \Omega(\cos\theta) f(\cos\theta) d(\cos\theta)$$
$$= \frac{\int_0^1 \Omega(\cos\theta) \exp\left[\sum_i (v_i/k_B T) \langle P_i \rangle P_i \right] d(\cos\theta)}{\int_0^1 \exp\left[\sum_i (v_i/k_B T) \langle P_i \rangle P_i \right] d(\cos\theta)}, \tag{3}$$

where $i=1$ and 2. Using Eq. (3), one can describe the equilibrium orientational order parameters for the ensemble of P_1 and P_2 ($\langle P_1 \rangle$ and $\langle P_2 \rangle$). Then the order parameters $\langle P_1 \rangle$ and $\langle P_2 \rangle$ appear on both the left and right hand sides of the equations, i.e., self-consistency conditions. Thus, for a given temperature T, one can obtain the values of $\langle P_1 \rangle$ and $\langle P_2 \rangle$ satisfying the self-consistency conditions by numerical calculation.

III. RESULTS AND DISCUSSION

First we calculated the polar order parameter $\langle P_1 \rangle$ and the axial order parameter $\langle P_2 \rangle$ as functions of $v_1/k_B T$ and $v_2/k_B T$ by using the self-consistency conditions [Eq. (3)]. From the obtained values of $\langle P_1 \rangle$ and $\langle P_2 \rangle$, we assigned the phase at $(v_2/k_B T, v_1/k_B T)$ as follows

$$\langle P_1 \rangle = 0 \quad \text{and} \quad \langle P_2 \rangle = 0 \rightarrow \textit{Iso},$$
$$\langle P_1 \rangle = 0 \quad \text{and} \quad \langle P_2 \rangle \neq 0 \rightarrow N,$$

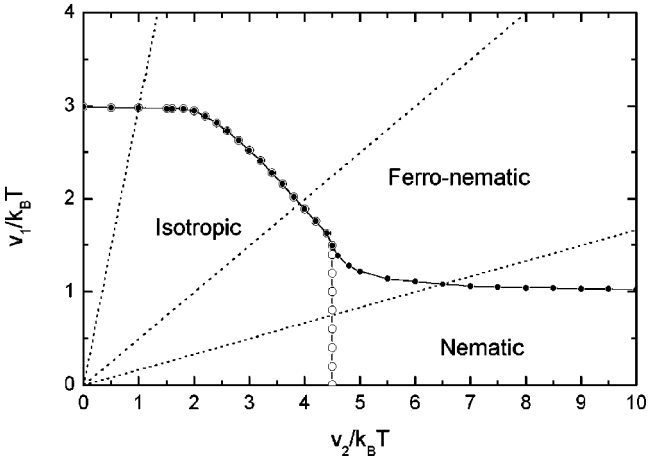

FIG. 1. The phase diagram in the $(v_2/k_B T, v_1/k_B T)$ plane obtained by solving the self-consistency conditions [Eq. (3)]. The open and filled circles represent the phase transition points monitored by the axial order parameter $\langle P_2 \rangle$ and the polar order parameter $\langle P_1 \rangle$, respectively. The dotted straight lines show the temperature paths for $v_1/v_2 = 3.0$, 0.5, and 0.165.

$$\langle P_1 \rangle \neq 0 \quad \text{and} \quad \langle P_2 \rangle \neq 0 \rightarrow \textit{FN},$$

where *Iso*, *N*, and *FN* refer to the isotropic, nematic, and ferroelectric nematic phases, respectively. Figure 1 shows the phase diagram obtained as a function of $v_2/k_B T$ and $v_1/k_B T$. As shown in the figure, one can clearly see *Iso*, *N*, and broad *FN* phases with the tricritical point among *Iso*, *N*, and *FN* phases at $(v_2/k_B T, v_1/k_B T) = (4.5, 1.5)$, indicating that the generalized potential predicts the existence of a *FN* phase for the high longitudinal dipole interaction over $v_1/k_B T \sim 1$. When the longitudinal dipole interaction is smaller than $v_1/k_B T \sim 1$, the normal *Iso-N* phase transition occurs at $v_2/k_B T \sim 4.54$, which is the same result as that obtained through the conventional mean-field theory for V_{axial}. Within the investigated region of $(v_2/k_B T, v_1/k_B T)$ in this study, the phase sequences can be distinguished for the ratio of (v_1/v_2) as follows:

$$0.00 \leqslant v_1/v_2 < 0.10, \quad \textit{Iso-N}, \quad \text{(I)}$$
$$0.10 \leqslant v_1/v_2 < 0.33, \quad \textit{Iso-N-FN}, \quad \text{(II)}$$
$$0.33 \leqslant v_1/v_2 < 1.65, \quad \textit{Iso-FN}, \ (1\text{st}) \quad \text{(III)}$$
$$1.65 \leqslant v_1/v_2 < \infty, \quad \textit{Iso-FN}, \ (2\text{nd}) \quad \text{(IV)}$$

Except for in region I, the phase sequences all show *FN* phase transitions. It is interesting to note that phase diagram is similar to that reported in ferromagnetic nematics [16,17]. Here, we would like to focus our attention on the *FN* phases related to the SHG response in regions II, III, and IV.

Now let us examine the phase transition behaviors as a function of reduced temperature $(k_B T/v_2)$ for the given ratios of $v_1/v_2 = 0.165$, 0.5, and 3. As shown by the dotted straight lines in Fig. 1, these values are representatives of regions II, III and IV, respectively. Figure 2(a) shows the investigated phase transition behaviors as a function of reduced temperature $(k_B T/v_2)$ for $v_1/v_2 = 0.165$. In the figure, the obtained order parameters $\langle P_1 \rangle$ and $\langle P_2 \rangle$ were plotted as

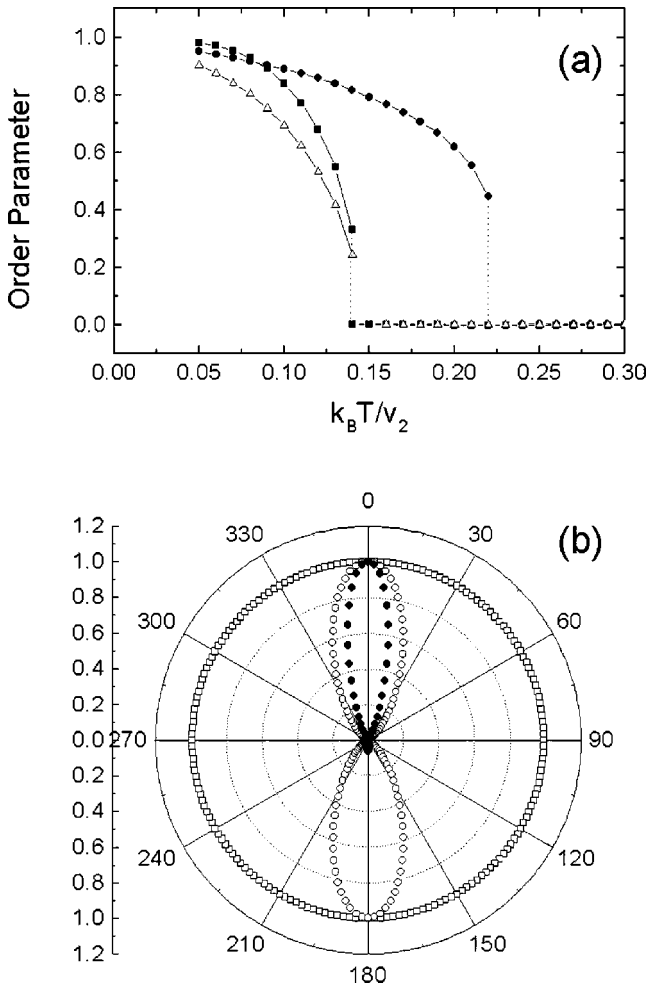

FIG. 2. (a) The order parameters $\langle P_1\rangle$ (filled squares), $\langle P_2\rangle$ (filled circles), and $\langle P_3\rangle$ (open triangles) as functions of reduced temperature (k_BT/v_2) for $v_1/v_2=0.165$. (b) The polar plots of the molecular distributions for $k_BT/v_2=0.3$ (open squares), 0.2 (open circles), and 0.1 (filled circles). 0° is defined as the $+\hat{n}$ director direction. The *FN* phase (filled circles) shows a larger probability toward parallel than antiparallel alignment.

filled squares and filled circles, respectively. As shown in the figure, for reduced temperatures k_BT/v_2 above $\sim$0.22, the isotropic phase becomes stable with $\langle P_2\rangle=\langle P_1\rangle=0$. At the clearing reduced temperature $k_BT/v_2\sim0.22$, one can see a first-order phase transition with the order parameter $\langle P_2\rangle$ changing abruptly from 0 to $\sim$0.43. In this region, $\langle P_1\rangle=0$, indicating that it is the *Iso-N* phase transition, which is the same feature as seen in the conventional mean-field model. At the reduced temperature of $k_BT/v_2\sim0.14$, however, one can clearly see another first-order phase transition with the order parameter $\langle P_1\rangle$ changing discontinuously from 0 to $\sim$0.33, while $\langle P_2\rangle$ increases continuously, namely the *N-FN* phase transition. As the reduced temperature k_BT/v_2 decreases from $\sim$0.14 to 0, the ferroelectric nematic phase is stable with $\langle P_1\rangle$ and $\langle P_2\rangle$ continuously increasing to unity. The phase sequence in this system can be written by

$$Iso(k_BT/v_2\sim0.22)N(k_BT/v_2\sim0.14)FN,$$

where all of the phase transitions are of the first order.

In the *FN* phase, the ferroelectricity of LC molecules can induce the second-order nonlinear optical (NLO) processes due to its noncentrosymmetric nature. Now, let us look at the second-order NLO coefficients $\chi^{(2)}$, which is responsible for SHG response ($\propto|\chi^{(2)}|^2$) [23]. The macroscopic NLO coefficients $\chi^{(2)}$ are related to the microscopic molecular contributions β as follows [23]

$$\chi^{(2)}_{IJK}=\sum N\beta_{ijk}\langle(I\cdot i)(J\cdot j)(K\cdot k)\rangle, \tag{4}$$

where N is the number density of molecule, (i,j,k) are the microscopic molecular coordinates, (I,J,K) are the macroscopic sample coordinates, and β_{ijk} is the molecular hyperpolarizability tensor. When the molecular chiral effect is neglected, the *FN* phase belongs to the $C_{\infty v}$ point group symmetry, and the nonzero $\chi^{(2)}$ components are $\chi^{(2)}_{333}$ and $\chi^{(2)}_{311}$, where $\hat{3}$ is the director direction $\hat{n}$. When the LC molecule is viewed as a one-dimensional molecule with the dominant molecular hyperpolarizability β_{zzz} along the long molecular axis z, the nonzero NLO coefficients are simply written as [24]

$$\begin{aligned}\chi^{(2)}_{333}&=\tfrac{1}{5}N(3\langle P_1\rangle+2\langle P_3\rangle)\beta_{zzz},\\ \chi^{(2)}_{311}&=\tfrac{1}{5}N(\langle P_1\rangle-\langle P_3\rangle)\beta_{zzz}.\end{aligned} \tag{5}$$

From the above relations, one can see that the another polar order parameter $\langle P_3\rangle$ in addition to the polar order parameter $\langle P_1\rangle$ is responsible for SHG response. The dependence of $\langle P_3\rangle$ obtained by the generalized mean-field description is also shown in Fig. 2(a) (open triangles) against reduced temperature for $v_1/v_2=0.165$. As shown in the figure, $\langle P_3\rangle$ begins to increase just when entering the *FN* phase. As the temperature decreases to zero, $(3\langle P_1\rangle+2\langle P_3\rangle)/5$ increases to unity continuously, but $(\langle P_1\rangle-\langle P_3\rangle)/5$ increases slightly and reaches a maximum followed by a significant decrease. Thus the dominant NLO coefficient is $\chi^{(2)}_{333}$ in the low temperature regime.

In order to see the changes in the molecular distributions, we also investigated the molecular (dipolar) distribution f as a function of the angle θ as shown in Fig. 2(b), where the distribution functions were normalized and polar plotted for convenience. For $k_BT/v_2=0.3$ (*Iso*), $f(\theta)$ clearly shows an isotropic distribution (open squares), while for $k_BT/v_2=0.2$ (*N*), $f(\theta)$ shows an anisotropic non-polar distribution (open circles), in which the orientational density in the $+\hat{n}$ direction is exactly the same as that in the $-\hat{n}$ direction, i.e., $f(\theta)=f(\pi-\theta)$. On the other hand, for $k_BT/v_2=0.1$ (*FN*), $f(\theta)$ shows an anisotropic polar distribution (filled circles), in which the orientational density in the $+\hat{n}$ direction is much higher than that in the $-\hat{n}$ direction. In this distribution, it is noted that the states $\hat{n}$ and $-\hat{n}$ are not equivalent, indicating the net dipole moment lies along $+\hat{n}$.

Next the phase transition behaviors for $v_1/v_2=0.5$ are shown in Fig. 3(a) as a function of reduced temperature. For reduced temperatures k_BT/v_2 above $\sim$0.25, the isotropic phase becomes stable with $\langle P_2\rangle=\langle P_1\rangle=0$. At the clearing

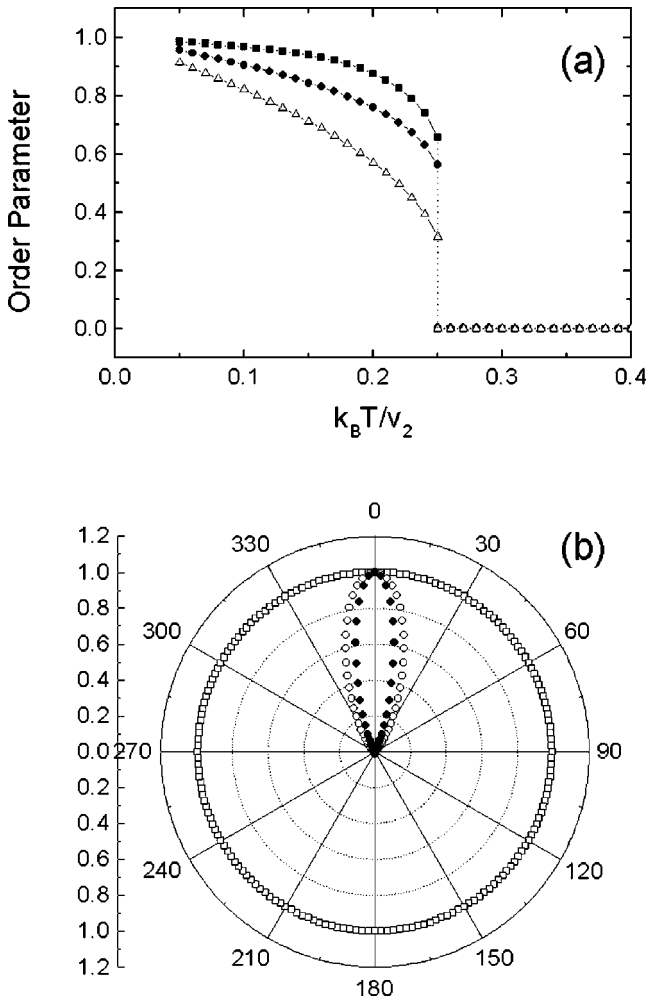

FIG. 3. (a) The order parameters $\langle P_1\rangle$ (filled squares), $\langle P_2\rangle$ (filled circles), and $\langle P_3\rangle$ (open triangles) as functions of reduced temperature (k_BT/v_2) for $v_1/v_2=0.5$. (b) The polar plots of the molecular distributions for $k_BT/v_2=0.3$ (open squares), 0.2 (open circles), and 0.1 (filled circles).

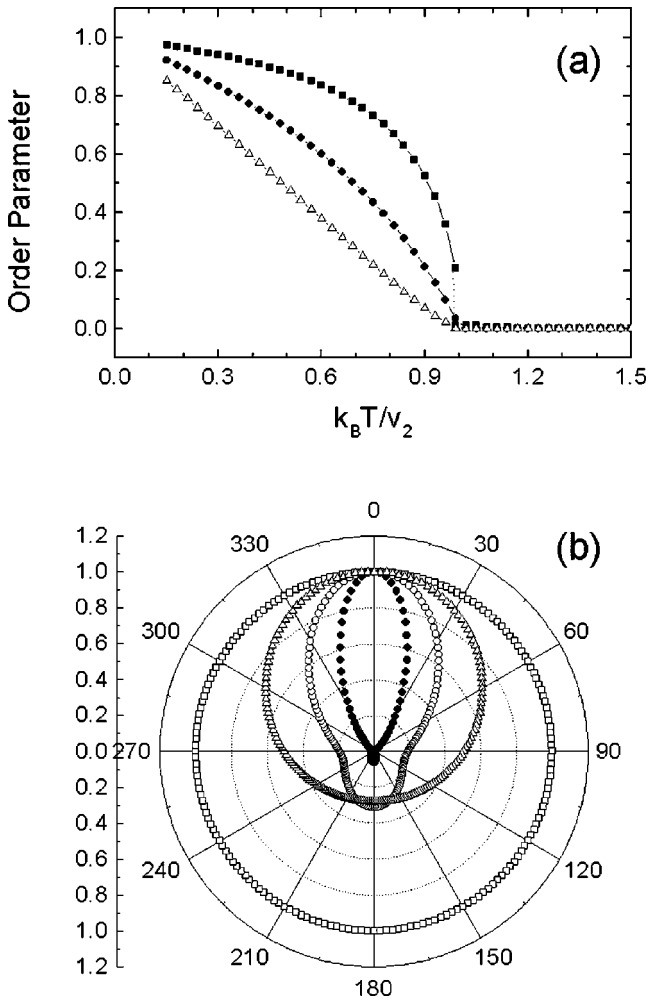

FIG. 4. (a) The order parameters $\langle P_1\rangle$ (filled squares), $\langle P_2\rangle$ (filled circles), and $\langle P_3\rangle$ (open triangles) as functions of reduced temperature (k_BT/v_2) for $v_1/v_2=3$. (b) The polar plots of the molecular distributions for $k_BT/v_2=1.2$ (open squares), 0.99 (open triangles), 0.9 (open circles), and 0.6 (filled circles).

reduced temperature $k_BT/v_2\sim0.25$, a first-order phase transition occurs. In this phase transition, $\langle P_2\rangle$ and $\langle P_1\rangle$ change discontinuously from 0 to ~0.56 and ~0.66, respectively. It is obviously the direct *Iso-FN* phase transition. As the reduced temperature k_BT/v_2 decreases from ~0.25 to 0, the ferroelectric nematic phase is stable with increasing $\langle P_1\rangle$ and $\langle P_2\rangle$ to unity continuously. The phase sequence in this system can be written

$$Iso(k_BT/v_2\sim0.25)FN,$$

where the phase transition is of the first order. The reduced temperature dependence of $\langle P_3\rangle$ is also shown for $v_1/v_2=0.5$ in Fig. 3(a). $\langle P_3\rangle$ begins to increase just when entering the *FN* phase. As the temperature decreases to zero, $(3\langle P_1\rangle+2\langle P_3\rangle)/5$ increases to unity continuously, but $(\langle P_1\rangle-\langle P_3\rangle)/5$ decreases continuously to zero. Thus, the dominant NLO coefficient is $\chi^{(2)}_{333}$ in the low temperature regime. The obtained molecular distribution functions for $k_BT/v_2=0.3$, 0.2, and 0.1 are shown in Fig. 3(b). For $k_BT/v_2=0.3$ (*Iso*), $f(\theta)$ shows the isotropic distribution, while for $k_BT/v_2=0.2$ (*FN*), $f(\theta)$ shows a polar nematic distribution, indicating that the net dipole moment lies along $+\hat{n}$. As k_BT/v_2 decreases to 0.1, the width of the polar distribution also decreases.

The phase transition behaviors were also investigated as a function of reduced temperature for $v_1/v_2=3$, as shown in Fig. 4(a). For reduced temperatures k_BT/v_2 above ~0.99, the isotropic phase becomes stable with $\langle P_2\rangle=\langle P_1\rangle=0$. At the clearing reduced temperature $k_BT/v_2\sim0.99$, one can see a phase transition; $\langle P_2\rangle$ changes continuously from 0, while $\langle P_1\rangle$ changes discontinuously from 0 to ~0.21. Thus, one can identify that it is another direct *Iso-FN* phase transition. As the reduced temperature k_BT/v_2 decreases from ~0.99 to 0, the ferroelectric nematic phase is stable with increasing $\langle P_1\rangle$ and $\langle P_2\rangle$ to unity continuously. The phase sequence in this system can be written

$$Iso(k_BT/v_2\sim0.99)FN,$$

where the $\langle P_1\rangle$ phase transition is of the first order and the $\langle P_2\rangle$ phase transition is of second order. The reduced temperature dependence of $\langle P_3\rangle$ for $v_1/v_2=3$ is also shown in Fig. 4(a). As shown in the figure, $\langle P_3\rangle$ begins to increase just when entering the *FN* phase. As the temperature decreases to zero, $(3\langle P_1\rangle+2\langle P_3\rangle)/5$ increases to unity continuously, but $(\langle P_1\rangle-\langle P_3\rangle)/5$ increases slightly and reaches a maximum followed by a significant decrease. Thus the dominant NLO coefficient is $\chi^{(2)}_{333}$ in the low temperature regime for all the ratios of v_1/v_2. These characteristics are useful for analyzing the SHG results in the *FN* liquid crystals consisting of molecules whose dominant hyperpolarizability is only β_{zzz}. The obtained molecular distribution functions for $k_BT/v_2=1.2$, 0.99, 0.9, and 0.6 are shown in Fig. 4(b). For $k_BT/v_2=1.2$ (*Iso*), $f(\theta)$ shows the isotropic distribution (open squares). For $k_BT/v_2=0.99$ at the *FN* phase transition, $f(\theta)$ shows a special distribution with zero value of $\langle P_2\rangle$ and nonzero value of $\langle P_1\rangle$, indicating a net dipole moment along director $+\hat{n}$ (open triangles). For the reduced temperature $k_BT/v_2=0.9$, $f(\theta)$ shows the trend of a polar nematic orientation of the *FN* phase (open circles). As k_BT/v_2 decreases to 0.6, the orientational distribution along $-\hat{n}$ decreases, and the width of the distributions also decreases (filled circles).

Next let us analyze the experimental SHG results for the cholesteric LC of poly *L*-glutamate [PBMLG, poly(γ-benzyl-*L*-glutamate-co-γ-methyl *L*-glutamate] reported previously [13], whose nonzero second-order NLO coefficients are $\chi^{(2)}_{333}=2.1\times10^{-10}$ esu and $\chi^{(2)}_{311}=-2.4\times10^{-10}$ esu, giving $\chi^{(2)}_{333}/\chi^{(2)}_{311}=-0.875$. The hyperpolarizability measurement of the poly *L*-glutamate molecule [25] suggests there exists a considerable contribution from β_{zxx} as well as β_{zzz} ($r_\beta=\beta_{zxx}/\beta_{zzz}=-0.8$); thus Eq. (5) should be modified as

$$\chi^{(2)}_{333}=\tfrac{1}{5}N[(3-2r_\beta)\langle P_1\rangle+2(1-r_\beta)\langle P_3\rangle]\beta_{zzz},$$
$$\chi^{(2)}_{311}=\tfrac{1}{5}N[(1+4r_\beta)\langle P_1\rangle-(1-r_\beta)\langle P_3\rangle]\beta_{zzz}. \quad (6)$$

In order to analyze the NLO coefficients, we used Lagrange's undetermined multipliers λ_is as $(v_i/k_BT\langle P_i\rangle)$s with the constraint functions of P_is, where $i=1$ and 2. Then the distribution function $f(\theta)$ can be rewritten by

$$f(\theta)=\frac{\exp\left[\sum_i \lambda_i P_i\right]}{\int \exp\left[\sum_i \lambda_i P_i\right] d(\cos\theta)}. \quad (7)$$

With the distribution f for given values of λ_is, one can calculate $\langle P_1\rangle$ and $\langle P_3\rangle$ using Eq. (3) and then, one can also calculate the NLO coefficients using Eq. (6). Thus, if one uses the λ_is as fitting parameters to the experimental results of $\chi^{(2)}$'s, then one can obtain the distribution function f with polar and axial order parameters. This process is similar to the maximum entropy method for obtaining the orientational distribution of adsorbed molecules from the experimental surface SHG results [26]. Following the analysis mentioned above, we obtained the best fit values of λ_i parameters: $\lambda_1=2.982$ and $\lambda_2=0.353$ to the experimental ratio of $\chi^{(2)}_{333}/\chi^{(2)}_{311}=-0.875$ for the PBMLG LC system. With these λ_i values, we obtained $\langle P_1\rangle=0.71$, $\langle P_2\rangle=0.40$, and $\langle P_3\rangle=0.19$ with the distribution f of PBMLG LC molecules, as shown in Fig. 5. The obtained order parameters and the polar orientation of PBMLG molecules shown in the figure clearly indicate that the PBMLG LC system has *FN* characteristics. We also estimated the hyperpolarizabilities for a PBMLG molecule by using Eq. (6) together with the molecular weight of ~200 000 (degree of polymerization $D_p\sim800$) and the number density of molecules $\sim1.8\times10^{18}$ molecules/cm^3; $\beta_{zzz}=3.52\times10^{-28}$ esu and $\beta_{zxx}=2.82\times10^{-28}$ esu. It is noted that these values are very close to $D_p\times\beta_{\text{monomer}}=1.6\times10^{-28}\pm50\%$ esu [27] for the poly (*L*-glutamate) molecule reported in dilute solution. Moreover, we also obtained additional important information about the ratio of the polar and the axial interaction potentials: $v_1/v_2=(\lambda_1/\langle P_1\rangle)/(\lambda_2/\langle P_2\rangle)=4.73$. Thus the PBMLG LC system has a *FN* phase in phase region IV. For $v_1/v_2=4.73$, $\langle P_1\rangle$ and $\langle P_2\rangle$ were estimated as a function of temperature. From the estimation, it was found that $(v_2/k_BT, v_1/k_BT)=(0.887, 4.167)$ gives $\langle P_1\rangle=0.71$ and $\langle P_2\rangle=0.40$, which are exactly the same as the values of ($\langle P_1\rangle=0.71$ and $\langle P_2\rangle=0.40$) for the PBMLG LC system. Thus one can estimate the axial and polar potentials of the PBMLG LC system as $v_2=0.887k_BT$ and $v_1=4.167k_BT$, respectively, at a temperature $T=300$ K.

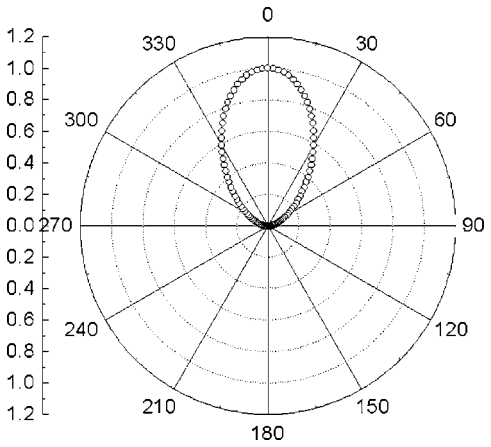

FIG. 5. The polar plot of the molecular distribution function $f(\theta)$ (open circles) obtained from $\chi^{(2)}_{333}/\chi^{(2)}_{311}=-0.875$ for the PBMLG LC system in Ref. [13].

Finally, we make a few comments on the above analysis for the PBMLG LC system. First, in the above analysis, the polar interaction potential may be overestimated, because we neglected the effect of the electric field applied to the system for investigating the field induced ferroelectric switching behaviors. The applied electric field may enhance the polar ordering. If one considers the electric field contribution to the generalized potential, then a more realistic analysis could be made. Second, the monitored SHG signals showed a long-term stability over 24 h with fairly large intensities of ~40%, even after the electric field was turned off. The long-term stability of the polar order cannot be explained by the relaxation behavior of the field induced polar order because the

temperature region of the LC phase is much higher than the glass transition temperature T_g (or the relaxation temperatures; $T_{\alpha,\beta,\gamma}$) for the poly (*L*-glutamate) systems [28]. Thus we can safely conclude that the SHG results for a PBMLG LC system can be explained only by using our mean-field theory for the *FN* phase. In this way, we have shown that the effective generalized mean-field theory can describe the ferroelectric nematic system, and suggested a way to analyze the experimental SHG results from the real system.

IV. CONCLUSION

We performed a self-consistent numerical analysis of the effective generalized mean-field potential, including axial and polar interaction potentials, and obtained a complete phase diagram of a liquid crystalline molecular system as a function of the axial and polar interaction potential strengths. The obtained phase diagram exhibits not only a typical isotropic nematic phase transition but also nematic ferroelectric nematic and direct isotropic-ferroelectric nematic phase transitions with a tricritical point at $(v_2/k_BT, v_1/k_BT) = (4.5, 1.5)$ among the phases. The phase transition behaviors and the angular orientational distribution function of the molecules were investigated by studying the dependence of the polar and axial order parameters on the reduced temperature. The polar order parameters $\langle P_1 \rangle$ and $\langle P_3 \rangle$ responsible for SHG were also investigated in the generalized mean-field potential description. For a concrete example, we performed a quantitative analysis of the SHG signal reported previously in a lyotropic poly *L*-glutamate system, detailing the relationship between the angular distribution function and the order parameters based on our potential model. This clarifies the nature of the ferroelectric phase responsible for SHG in nematics.

This study can be easily generalized to the studies of various ferroelectric structures appearing in polymeric liquid crystal systems such as the thermotropic poly *L*-glutamate LC system and the aromatic copolyester LC system. Moreover, this study can provide basic information to further detailed theoretical studies of molecular interactions.

ACKNOWLEDGMENTS

The authors would like to thank Dr. D. Link for a careful reading of the manuscript. This work was supported by Brain Korea 21 project, KAIST (CAFPoly)-TIT core university program, and Korea Research Foundation Grant No. (KRF-2000-015-DP0151).

[1] R. B. Meyer, L. Liebert, L. Strzelecki, and P. Keller, J. Phys. (France) Lett. **36**, L69 (1975).
[2] A. D. L. Chandani, Y. Ouchi, H. Takezoe, A. Fukuda, K. Terashima, K. Furukawa, and A. Kishi, Jpn. J. Appl. Phys. **28**, L1261 (1989).
[3] T. Niori, T. Sekine, J. Watanabe, T. Furukawa, and H. Takezoe, J. Mater. Chem. **6**, 1231 (1996).
[4] H. Takezoe and J. Watanabe, Mol. Cryst. Liq. Cryst. **328**, 325 (1999).
[5] P. Palffy-Muhoray, M. A. Lee, and R. G. Petschek, Phys. Rev. Lett. **60**, 2303 (1988).
[6] D. Wei and G. N. Patey, Phys. Rev. Lett. **68**, 2043 (1992).
[7] M. Baus and J. L. Colot, Phys. Rev. A **40**, 5444 (1989).
[8] E. M. Terentjev, M. A. Osipov, and T. J. Sluckin, J. Phys. A **27**, 7047 (1994).
[9] J. Lee and S.-D. Lee, Mol. Cryst. Liq. Cryst. **254**, 395 (1994).
[10] T. Furukawa, K. Ishikawa, H. Takezoe, A. Fukuda, T. Watanabe, S. Miyata, T. Nishi, M. Sone, and J. Watanabe, Nonlinear Opt. **15**, 167 (1996).
[11] T. Furukawa, H. Takezoe, T. Nishi, T. Mitsukuchi, A. Migita, J. Watanabe, T. Watanabe, and S. Miyata, Mol. Cryst. Liq. Cryst. **299**, 105 (1997).
[12] T. Watanabe, S. Miyata, T. Furukawa, H. Takezoe, T. Nishi, M. Sone, A. Migita, and J. Watanabe, Jpn. J. Appl. Phys. **35**, L505 (1996).
[13] B. Park, Y. Kinoshita, H. Takezoe, and J. Watanabe, Jpn. J. Appl. Phys. **37**, L136 (1998).
[14] S. Chandrasekhar and N. V. Madhusudana, Acta Crystallogr., Sect. A: Cryst. Phys., Diffr., Theor. Gen. Crystallogr. **27**, 303 (1971).
[15] R. L. Humphries, P. G. James, and G. R. Luckhurst, J. Chem. Soc., Faraday Trans. 2 **68**, 1031 (1972).
[16] I. C. Teixeira, Liq. Cryst. **25**, 721 (1998), and references therein.
[17] A. Oukouiss and M. Baus, J. Chem. Phys. **109**, 6157 (1998).
[18] J. M. Tavares, M. M. Telo da Gama, P. I. C. Teixeira, J. J. Weis, and M. J. P. Nijmeijer, Phys. Rev. E **52**, 1915 (1995).
[19] P. J. Wojtowicz, in *Introduction to Liquid Crystal*, edited by E. B. Priestley, P. J. Wojtowicz and P. Sheng (Plenum, New York, 1979), p. 45, and references therein.
[20] W. Maier and A. Saupe, Z. Naturforsch., A: Phys. Sci. **13**, 564 (1959); **14**, 882 (1960); **15**, 287 (1960).
[21] S. Chandrasekhar, in *Liquid Crystal* (Cambridge University Press, London, 1977), p. 84.
[22] A. V. Emelyanenko and M. A. Osipov, Liq. Cryst. **26**, 187 (1999).
[23] D. J. Williams, in *Nonlinear Optical Properties of Organic Molecules and Polymers*, edited by D. S. Chemla and J. Zyss (Academic, New York, 1987), p. 405, and references therein.
[24] J. W. Wu, J. Opt. Soc. Am. B **8**, 142 (1991).
[25] From the hyper-Rayleigh scattering measurement, details will be reported elsewhere.
[26] B. Park, Y. Kinoshita, T. Sakai, J.-G. Yoo, H. Hoshi, K. Ishikawa, and H. Takezoe, Phys. Rev. E **57**, 6717 (1998).
[27] B. F. Levine and C. G. Bethea, J. Chem. Phys. **65**, 1989 (1976).
[28] J. Watanabe, H. Ono, I. Uematsu, and A. Abe, Macromolecules **18**, 2141 (1985).